scientific reports

OPEN

NIR self-powered photodetection and gate tunable rectification behavior in 2D GeSe/MoSe$_2$ heterojunction diode

Muhammad Hussain[1], Syed Hassan Abbas Jaffery[1], Asif Ali[1], Cong Dinh Nguyen[1], Sikandar Aftab[2], Muhammad Riaz[1], Sohail Abbas[3], Sajjad Hussain[1], Yongho Seo[1] & Jongwan Jung[1✉]

Two-dimensional (2D) heterostructure with atomically sharp interface holds promise for future electronics and optoelectronics because of their multi-functionalities. Here we demonstrate gate-tunable rectifying behavior and self-powered photovoltaic characteristics of novel p-GeSe/n-MoSe$_2$ van der waal heterojunction (vdW HJ). A substantial increase in rectification behavior was observed when the devices were subjected to gate bias. The highest rectification of $\sim 1 \times 10^4$ was obtained at V$_g$ = – 40 V. Remarkable rectification behavior of the p-n diode is solely attributed to the sharp interface between metal and GeSe/MoSe$_2$. The device exhibits a high photoresponse towards NIR (850 nm). A high photoresponsivity of 465 mAW^{-1}, an excellent EQE of 670%, a fast rise time of 180 ms, and a decay time of 360 ms were obtained. Furthermore, the diode exhibits detectivity (D) of 7.3×10^9 Jones, the normalized photocurrent to the dark current ratio (NPDR) of 1.9×10^{10} W^{-1}, and the noise equivalent power (NEP) of 1.22×10^{-13} WHz$^{-1/2}$. The strong light-matter interaction stipulates that the GeSe/MoSe$_2$ diode may open new realms in multi-functional electronics and optoelectronics applications.

Beyond the great success of graphene and their derivatives, the analogs of the 2D materials, such as the transition metal dichalcogenide (TMD) and the transition metal carbide (TMC) nanostructures have strikingly increased interest in science. Compared to graphene, which has high carrier mobility but zero bandgap limited its device application, and the transition-metal dichalcogenides (TMDs) that have the formula MX$_2$ (M = Mo, W, Ge; X = S, Se, or Te), a class of 2D semiconductors have recently attracted remarkable scientific and technological interest for innovative devices. They exhibit a wide range of material properties, such as high carrier mobility for both electrons and holes, have a relatively large bandgap of 1.5–2.5 eV, have a tunable direct bandgap that ranges from 0.3 to 1.5 eV, have an ideal sub-threshold swing of ~ 60 mV/dec, an I$_{ON}$/I$_{OFF}$ ratio of 10^8–10^9, and high carrier mobility (200 cm^2 V^{-1} s^{-1}@ room temperature mobility for a single-layer MoS$_2$ transistor with high-K dielectric and 1000 cm^2 V^{-1} s^{-1}@ 3 K temperature)[1–3]. Due to the weak van der Waals interface forces in graphene and TMDs materials, the p–n diode or the Schottky barriers (SBs) at the metal/TMDs interfaces have played an important role in electronic devices[4]. Besides, the electrical properties are hindered by the contact resistances rather than the intrinsic TMDs properties. The development of the TMDs with different bandgaps and work functions allow for the bandgap engineering of heterostructures that may possess new physical and electrical properties. Among TMDs materials, which include MoSe$_2$, GeS, and GeSe, have been proposed as alternative 2D systems, and they have exhibited better performance in photodetectors. GeSe belongs to the layered IV–VI nanostructures since the p-type semiconductors with narrow bandgap (1.1–1.2 eV) are potential alternatives to the lead chalcogenides and open an avenue to fabricate highly efficient electronic and optoelectronic devices[5,6]. The MoSe$_2$ from indirect (bulk crystal) to direct (monolayer) results in the bandgap increasing from 1.1 to 1.5 eV, which become direct in single atomic layers, and it makes them promising candidates in field-effect transistors (FETs), photovoltaic cells, light-emitting diodes (LEDs), and photodetectors. With the lower light response in photodetection/sensing, the bandgap tunability value for electrons or hole transfers between bulk TMDs materials down to the monolayer and slow electron transfer pathways is still greatly impeded. Consequently,

[1]Department of Nanotechnology and Advanced Materials Engineering, and HMC, Sejong University, Seoul 05006, South Korea. [2]Department of Engineering, Simon Faster University, Burnaby, Canada. [3]Faculty of Engineering and Applied Sciences, Ripah International University, Islamabad, Pakistan. ✉email: jwjung@sejong.ac.kr

1

consideration will still be given to matching the band alignment for electron or hole transfers between bulk materials for the development of photodetector creation.

By combing two semiconductors, the study of heterojunctions with the same lattice structures has become a hot topic in semiconductor technology. Recently, scientists have paid a great deal of attention to fabricating heterojunctions on graphene-like materials or heterojunctions by combining two semiconductors/semimetals, such as graphene-h-BN[7], graphene-MoS$_2$[8,9], and graphene-MoSe$_2$[10–12]. On the other hand, some heterojunctions are designed based on TMDs materials, which include [2D/2D] structures via either mechanical exfoliation or vapor deposition methods that include MoSe$_2$/WSe$_2$ heterojunction[13], MoSe$_2$/WS$_2$ heterostructures[14], MoS$_2$/black phosphorus heterojunction[15], p-type GaSe/n-type MoSe$_2$[16], [2D/1D] black phosphorus–zinc oxide nanomaterial heterojunction[17,18], n-2D/p-oxide, and p-2D/n-oxide structures[17,19–21], such as vertical MoSe$_2$-MoO$_x$[22].

These novel semiconducting [2D/2D] TMDs/TMDs are now a primary focus of many researchers. Several TMDs based materials are under fabrication process to explore new physics and the next-generation photonic/optoelectronic devices. In the present study, we demonstrated the p-GeSe/n-MoSe$_2$ heterojunction self-powered photodiodes. We observed good gate-tunable rectification characteristics of the p-GeSe/n-MoSe$_2$ heterojunction p-n diode. The high ratification ratio of 1.4×10^4 is obtained at $V_{bg} = -40$ V. The photovoltaic behavior of the p-GeSe/n-MoSe$_2$ heterojunction p-n diode at zero bias was investigated under various intensities of (53.3, 98.5, 123, and 139 mW/cm^2) with NIR (850 nm) incident photons. The high responsivity (R = 465 mAW^{-1}), the detectivity D of 7.3×10^9 Jones, the normalized photocurrent to dark current ratio NPDR of 1.9×10^{10} W^{-1}, the noise equivalent power NEP of 1.22×10^{-13} WHz$^{-1/2}$, and the external quantum efficiency EQE of 670% were observed with a fast response time of 180 ms. The strong light-matter interaction in the device explicitly suggests that the p-GeSe/n-MoSe$_2$ heterojunction p–n diode is a promising candidate for optoelectronics technologies.

Experimentation

We prepared all the p-GeSe and the n-MoSe$_2$ atomically thin flakes by peeling them from their parent bulk crystals using a scotch tape mechanical exfoliation technique, which is similar to the technique that is employed for the exfoliation of graphene[23,24], and we transferred it onto a Si/SiO2 (300 nm) substrate using a transparent poly (dimethylsiloxane) (PDMS) stamp using an aligned dry transfer[25,26]. The multilayer p-GeSe and the n-MoSe$_2$ flakes were identified using an optical microscope, and the multilayer n-MoSe$_2$ was directly stacked on the top of the p-GeSe flake. Raman spectroscopy and atomic force microscopy (AFM) were also conducted. Electron beam lithography was used for the metal deposition of palladium/gold (Pd/Au:10/20 nm) and (Cr/Au:10/20 nm) onto the p-GeSe and the n-MoSe2, respectively. The lift-off processes were conducted to form electrodes on the multilayer p-GeSe and n-MoSe2 flakes. The electrical characterization at room temperature were exhibited using a Keithley 4200A-SCS parameter analyzer. The photovoltaic characteristics of the p-GeSe/n-MoSe$_2$ heterojunction photodetector was performed using a continuous wave laser beam from a diode NIR laser (850 nm) that was directly illuminated onto the device.

Result and discussions

A schematic illustration of the demonstrated p-GeSe/n-MoSe$_2$ heterostructure device is depicted in Fig. 1a. The optical image of the p-GeSe/n-MoSe$_2$ heterostructure is shown in Fig. 1b. The atomically thin flakes of the p-GeSe and the n-MoSe$_2$ were peeled from their parent bulk crystals using a scotch tape mechanical exfoliation technique, which was transferred on a 300 nm SiO$_2$/Si substrate[27]. A few-layers of the n-MoSe$_2$ were directly stacked on the top of the p-GeSe nanoflake by precisely determining their locations and an overlapping heterojunction region was formed. To clean the surface and optimize the charge carrier, the flakes of the p-GeSe and the n-MoSe$_2$ were annealed at 200 °C for 1 h in an argon environment[28]. The Pd/Au (10/20 nm) and the Cr/Au (10/20 nm) optimum metal electrodes were then designed onto the p-GeSe and the n-MoSe2 flakes. Figure 1c–f shows the thickness of the p-GeSe (n-MoSe$_2$), which is ~ 8 nm (~ 6 nm), and their height profiles that were measured by the atomic force microscopy (AFM) analysis. Raman spectroscopy was used to confirm the material p-type GeSe and the n-type MoSe$_2$ shown in Figure S1(a). The p-GeSe/n-MoSe$_2$ heterostructure device was electrically characterized at room temperature by applying drain to source voltage (V_{ds}) and electrostatic back-gate voltage (V_g). To validate the doping nature of the material GeSe and MoSe$_2$, the back-gate voltage (V_g) was swept from − 40 to + 40 V at constant $V_{ds} = 2$ V, and the transfer characteristics revealed that the material GeSe (MoSe$_2$) exhibited a p-type (n-type) nature with an ON/OFF ratio of $2.42 \times 10^3 (1.28 \times 10^3)$, which is depicted in Fig. 2a, b. The semiconductor material and the metal interface could exhibit either ohmic behavior or rectifying behavior depending on the semiconductor and the metals working function values. Hence, we used optimum metal contacts for Pd ($\Phi \sim 5.6$ eV)[29] Cr ($\Phi \sim 4.5$ eV) p-GeSe(n-MoSe$_2$)[30,31]. Figure 2c shows ohmic behavior with a high work function of the Pd. To induce ohmic behavior between the metal and the n-MoSe$_2$, we used the low work function of the Cr depicted in Fig. 2d. The field-effect carrier mobility (μ_{FE}) of the p-GeSe and the n-MoSe$_2$ was calculated using the following equation[32–34].

$$\mu_{FE} = \frac{L}{W} \left(\frac{dI_{ds}}{dV_{bg}} \right) \frac{1}{C_{bg} V_{ds}} \tag{1}$$

where W is the channel width, L is the channel length, C_{bg} is the gate capacitance (~ 115 aF/μm^2) for the SiO$_2$ substrate, and ($\frac{dI_{ds}}{dV_{bg}}$) is the slope of the transfer curve. The mobilities of the p-GeSe and the n-MoSe$_2$ were estimated to be 110 cm^{2}V^{-1} s^{-1} and 85 cm^{2}V^{-1} s^{-1}, respectively.

The gate-tunable electrical characteristics were also investigated. Figure 3a exhibits the gate dependent output characteristics of the p-GeSe/n-MoSe$_2$ heterostructure diode, and Fig. 3b shows the same output curves in a corresponding logarithmic plot. It revealed that the rectifying behavior of the device is tuned by the electrostatic
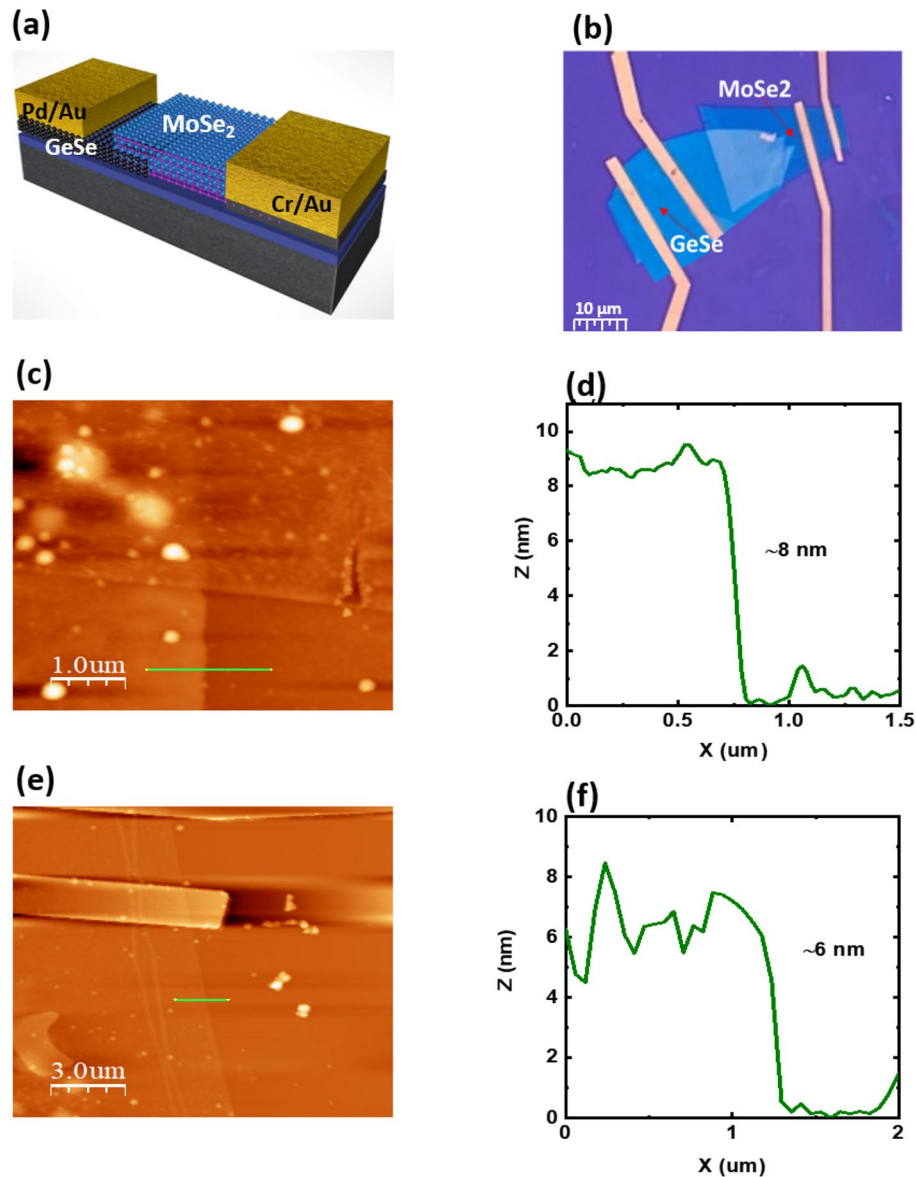
Figure 1. (a) A schematic view of the p-GeSe/n-MoSe$_2$ heterojunction diode. (b) The optical microscope image of the device. (c) An AFM image of the p-GeSe on the SiO$_2$/Si substrate. (d) The height profile from the AFM. (e) An AFM image of n-MoSe$_2$ on the SiO$_2$/Si substrate, and (f) their height profile.

gate-voltage. The forward bias rectifying current increases as the gate voltages (V_g) increased from $-V_g$ to $+V_g$, the electrons are attracted to the interface between GeSe and SiO$_2$ to form accumulation layer results the Fermi level of GeSe moves towards the conduction band and lowering potential barrier height results in decreasing rectification current attributed to electrostatic doping of electrons. Moreover, we investigated the rectification ratio, which is defined as the ratio of the forward current over the reverse current, I_f/I_r, up to 1.4×10^4 at $V_g = -40$ V. We found that at a positive gate voltage of $V_g = +40$ V, both the reverse and forward currents increase concurrently, which suppress the rectification as a result. In anticipation of the negative gate voltage, the reverse current is constrained to increase the rectification in the p-GeSe/n-MoSe$_2$ heterostructure diode, which is depicted in Fig. 3c. Additionally, we estimated the ideality factor to confirm the performance of the rectifying behavior of the p-GeSe/n-MoSe$_2$ heterojunction diode using the thermionic emission theory[4,35].

$$I_D = I_S \left[\exp\left(\frac{qV}{nK_BT} \right) - 1 \right] \qquad (2)$$

where I_S is the reverse bias saturation current, n is the ideality factor, q is the elementary charge, T is the temperature, and K_B is Boltzmann's constant. After the interpretation above, the equation becomes
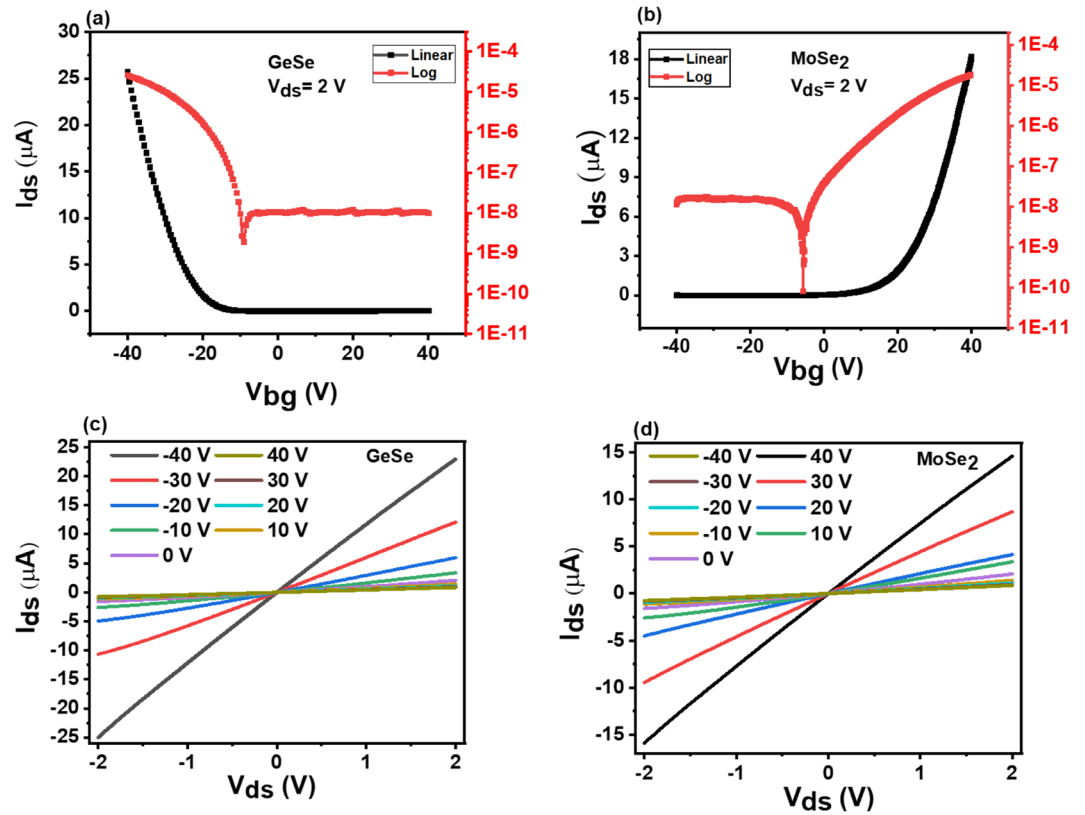
Figure 2. (a) The transfer characteristics of p-GeSe. (b) n-MoSe$_2$. (c) The linear $I_{ds}-V_{ds}$ curves of p-GeSe shows ohmic behavior with Pd/Au, and (d) the linear $I_{ds}-V_{ds}$ curves of n-MoSe$_2$ also show ohmic behavior with Cr/Au.

$$ln(I_D) = ln(I_S) + \left(\frac{q}{nK_BT}\right)V \tag{3}$$

The ideality factor (n) can be obtained via the following equation.

$$n = \left(\frac{q}{K_BT}\right) \Big/ \left(\frac{dV}{dlnI_D}\right) \tag{4}$$

Figure 3d illustrates the ideality factor function of the gate voltage, the ideality factor of 1.1 is obtained at $V_g = -40$ V, which is close to the ideal diode value ($\eta = 1$). The relative degrading of the gate tunable ideality factor is attributed to the surface carrier recombination at the interface of the p-GeSe/n-MoSe$_2$ diode, which results in a decrease in the electric field[21]. The variation in the electron affinity and the bandgap between the monolayers generates an atomically sharp hetero-interface, and the interface band alignment of the p-GeSe/n- MoSe$_2$ heterostructure is predicted to be a type II band alignment, which is shown in Fig. 4.

Furthermore, we investigated the self-powered photovoltaic characteristics of a p-GeSe/n-MoSe$_2$ heterostructure device. The self-powered photodetectors are devices that can separate photoexcited carriers by the built-in electrical field at the junctions without any external power source. On this principle, the p-n junctions can be established for the photovoltaics[36,37]. We used an NIR (850 nm) laser with various illumination power intensities (53.3, 98.5, 123, and 139 mW/cm^2) to measure the photocurrent generated from the photodiode that was based on the p-GeSe/n-MoSe$_2$ heterojunction. A strong photoresponse was observed in the p-GeSe/n-MoSe$_2$ junction region, which showed that a continuous charge separation occurred at the junction. Figure 5a presents the $I_{ds}-V_{ds}$ curves of the p-GeSe/n-MoSe$_2$ heterojunction in dark and under photon irradiation with wavelength of 850 nm at zero bias with a constant gate voltage ($V_g = 0$). The $I_{ds}-V_{ds}$ curves are shifted down under the irradiation of light, which revealed that the device can be developed for self-powered photovoltaic energy conversion under the action of open-circuit voltage (V$_{oc}$). We investigated an open-circuit voltage (V$_{oc}$) of 0.349 V and a short-circuit current (I$_{sc}$) of 14.5 nA for the 139 mW cm^{-2} light intensity. The external quantum efficiency (EQE) was investigated by using the following formula.

$$EQE = \frac{hc}{e\lambda}R \tag{5}$$

where λ is the incident light wavelength, h is the planks constant, and c is the velocity of light. We obtained a value for EQE of 670% in the p-GeSe/n-MoSe$_2$ diode. The power intensity-dependent EQE is depicted in Fig. 5b.
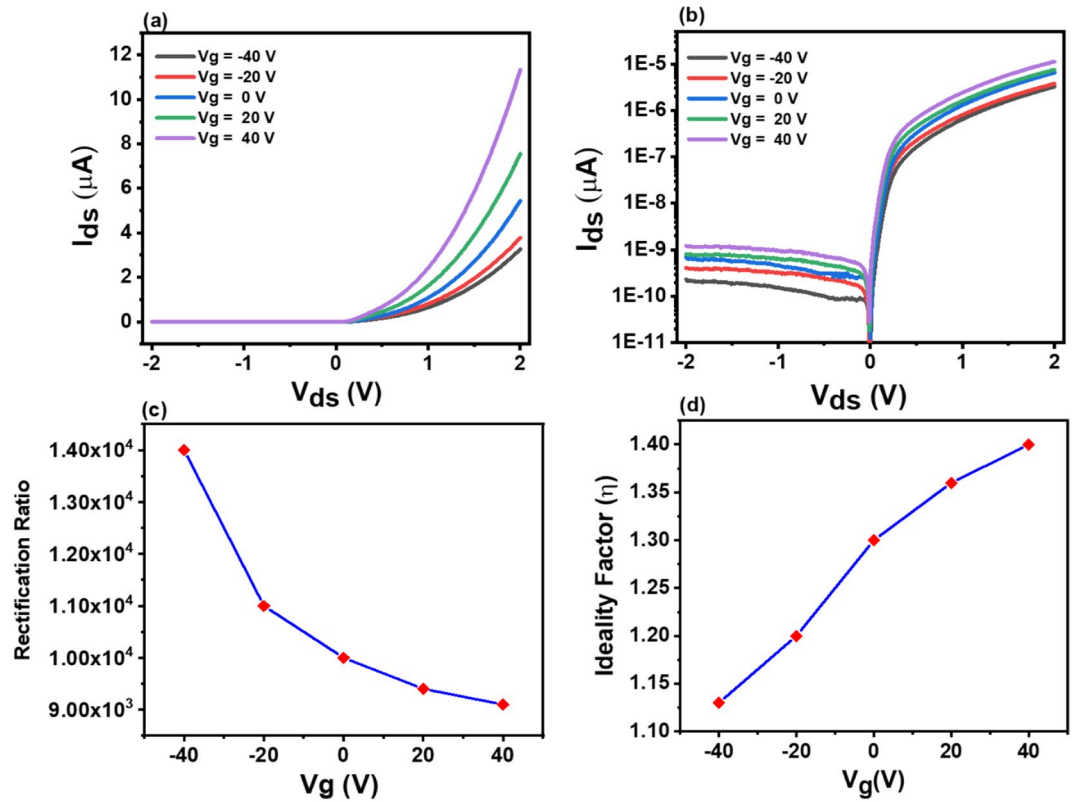
Figure 3. (**a**) The *I–V* characteristics of the p-GeSe/n-MoSe$_2$ heterojunction diode at different gate voltages. (**b**) The corresponding semi-logarithmic plots of output characteristics. (**c**) The gate dependent rectification ratio of p-GeSe/n-MoSe$_2$ heterojunction diode. (**d**) Gate dependent ideality factor of p-GeSe/n-MoSe$_2$ heterojunction diode.
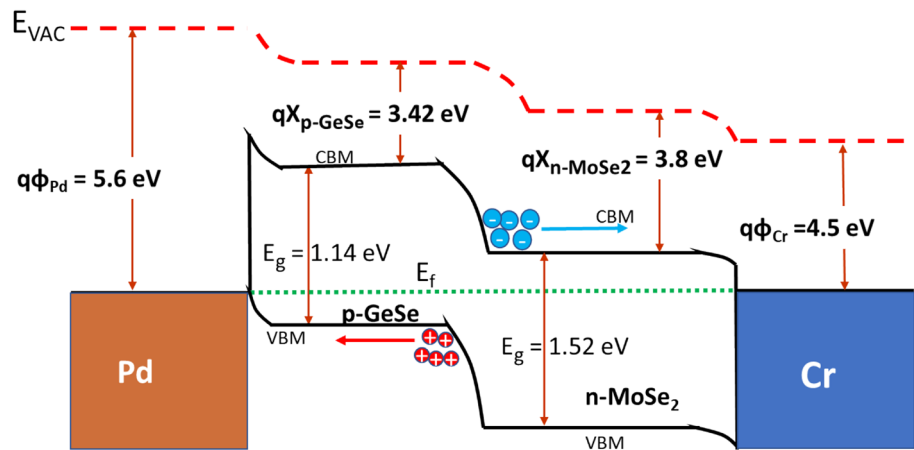

Figure 4. The band diagram of p-GeSe/n-MoSe$_2$ heterojunction diode with metal electrodes.

Additionally, we also characterized the transient photoresponse of the device. The dynamic photoresponse rise and fall time of the p-GeSe/n-MoSe$_2$ diode was observed under an NIR laser light irradiation with a wavelength (λ) of 850 nm at various power intensities, which is shown in Fig. 5c. The rise time is the τ_r, the time it takes by the device to reach 90% from 10% and the fall time is τ_f, the time it takes by the device to decay from 90 to 10%[36,38,39]. We found a rise time of 180 ms and a fall time of 360 ms, which are shown in Fig. 5d. The response time of the device is not as fast as we expected, which may be due to the charge carrier trapping and the longer charge dissociation time[40–42].

Moreover, in order to evaluate the performance of the device, several important figures of merits were calculated. For example, responsivity (R), detectivity (D), the normalized photocurrent to a dark current ratio (NPDR), and the noise equivalent power (NEP) with variation of incident light power intensities were calculated. The
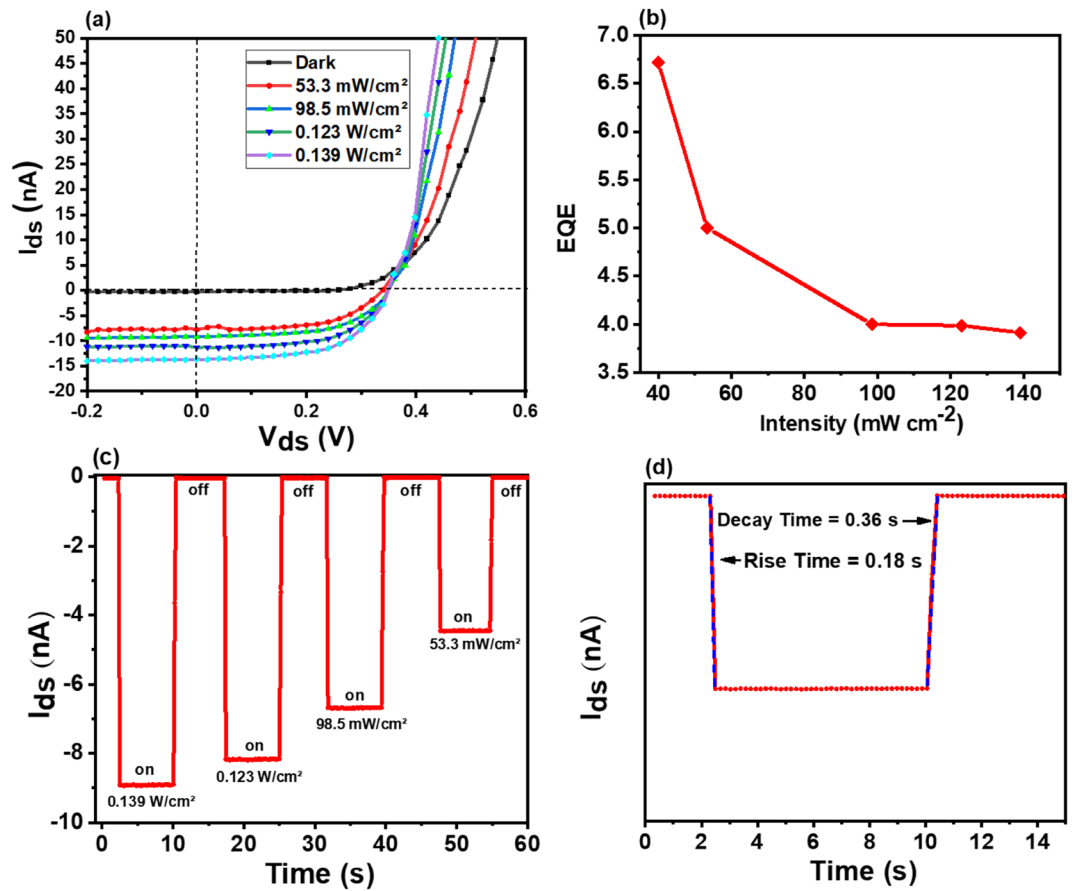
Figure 5. (a) The I–V characteristics of p-GeSe/n-MoSe$_2$ heterojunction diode under dark and variable intensities. (b) The external quantum efficiency EQE function of incident power. (c) The time-dependent photoresponse of p-GeSe/n-MoSe$_2$ heterojunction diode under illuminations with different laser light (@850 nm) intensity at $V_{ds}=0$ V. (d) The rise time and decay time.
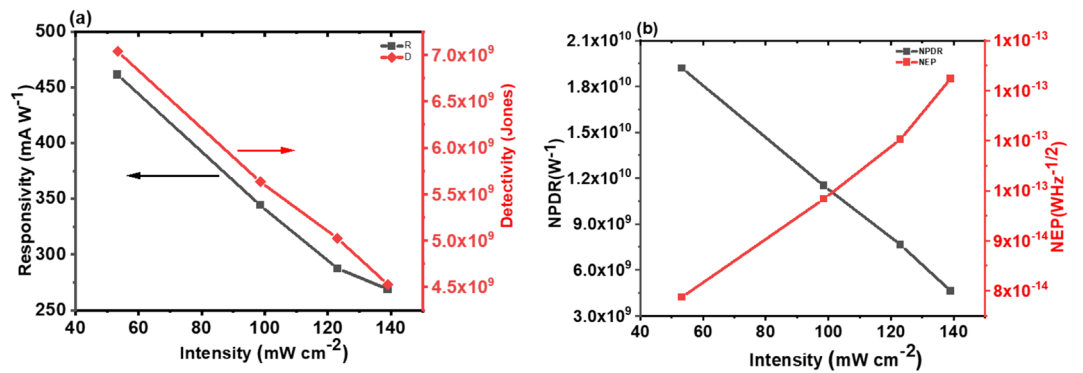

Figure 6. (a) The responsivity, R (mA W^{-1}), and the detectivity, D (Jones) function of power intensities (b) the normalized photocurrent to dark current ratio NPDR (W^{-1}) and the noise equivalent power NEP (W Hz$^{-1/2}$) function of power intensities.

responsivity ($R = J_p/P_{in}$), where J_p is the photocurrent density and P_{in} is input power per area, and the detectivity ($D = R/\sqrt{2qJ_d}$), where q is the elementary charge and J_d is the dark current density, are significant facets of the photo detector[36,38,39] , which is shown in Fig. 6a. The greater value of responsivity is attributed to the higher photocurrent[43]. Similarly, the device that has a lower dark current provides a higher detectivity. Thus, the greater values of both R and D are important aspects of an efficient photodetector[37,43,44]. We obtained a high responsivity of R = 465 mAW^{-1} and detectivity of D = 7.3 × 10^9 Jones.

Figure 6b shows the intensity-dependent normalized photocurrent to dark current ratio. The $NPDR = R/I_d$, where R is the responsivity, I_d is the dark current, and the noise equivalent power (NEP = $1/(NPDR\sqrt{2q/I_d})$). We investigated the values of NPDR of 1.9×10^{10} W^{-1} and NEP of 1.22×10^{-13} WHz$^{-1/2}$ under the power intensity of 139 mW cm^{-2}. The NEP revealed that the photodetector, which is based on the p-GeSe/n-MoSe$_2$ heterostructure, has the capability of detecting power as low as 10^{-13}. Additionally, we characterized the spectral responsivity of the p-GeSe/n-MoSe2 heterojunction. The device was subjected to constant illuminating power of 53 mW cm^{-2} with wavelength ranging from 220 to 850 nm. Figure S1c shows a sharp increase of the spectral response on the short wavelength side is reasonably due to more photon energy absorbed by the device, attributed to more electrons and holes generation under larger photons energy. Table S1 in supplementary information shows the comparative investigated photoresponse and sensitivity of our device based on p-GeSe/n-MoSe$_2$ heterojunction, which is much higher than the previously reported values. The strong light-matter interaction in the device explicitly suggests that the p-GeSe/n-MoSe$_2$ heterojunction p–n diode is a promising candidate for optoelectronics technologies.

Conclusions

In summary, we demonstrate a p-GeSe/MoSe$_2$ based multifunctional HJ p–n diode. The diode explicitly exhibits gate tunable high rectification of ~ 1×10^4 at negative gate bias (Vg = − 40 V). The introduction of the ohmic contacts reveals that the rectification behavior of a p–n diode is solely attributed to the sharp interface between metal contacts and GeSe/MoSe$_2$. Our device shows high photoresponse at an NIR (850 nm). The high responsivity of 465 mAW^{-1}, the excellent EQE (670%), the fast rise time of 180 ms, and the decay time of 360 ms were obtained. The device also shows detectivity D of 7.3×10^9 Jones, a normalized photocurrent to dark current ratio NPDR of 1.9×10^{10} W^{-1}, and a noise equivalent power NEP of 1.22×10^{-13} WHz$^{-1/2}$. The NEP revealed that the photodetector, which is based on the p-GeSe/n-MoSe$_2$ heterostructure, has the capability of detecting power as low as 10^{-13}. These results suggest that p-GeSe/MoSe$_2$ based multifunctional heterojunction p–n diode may have great potential for electronics and optoelectronics applications as high-performance self-powered photodetectors.

References

1. Fang, H. *et al.* Degenerate n-doping of few-layer transition metal dichalcogenides by potassium. *Nano Lett.* **13**(5), 1991–1995 (2013).
2. Lopez-Sanchez, O., Lembke, D., Kayci, M., Radenovic, A. & Kis, A. Ultrasensitive photodetectors based on monolayer MoS 2. *Nat. Nanotechnol.* **8**(7), 497 (2013).
3. Fuhrer, M. S. & Hone, J. Measurement of mobility in dual-gated MoS 2 transistors. *Nat. Nanotechnol.* **8**(3), 146 (2013).
4. Hussain, M. *et al.* Asymmetric electrode incorporated 2D GeSe for self-biased and efficient photodetection. *Sci. Rep.* **10**(1), 9374 (2020).
5. Vaughn, D. D., Patel, R. J., Hickner, M. A. & Schaak, R. E. Single-crystal colloidal nanosheets of GeS and GeSe. *J. Am. Chem. Soc.* **132**(43), 15170–15172 (2010).
6. Makinistian, L. & Albanesi, E. Ab initio calculations of the electronic and optical properties of germanium selenide. *J. Phys. Condens. Matter* **19**(18), 186211 (2007).
7. Dean, C. R. *et al.* Boron nitride substrates for high-quality graphene electronics. *Nat. Nanotechnol.* **5**(10), 722 (2010).
8. Yu, L. *et al.* Graphene/MoS2 hybrid technology for large-scale two-dimensional electronics. *Nano Lett.* **14**(6), 3055–3063 (2014).
9. Graphene-assisted epitaxy of group IV semiconductor nanostructures and thin films. in *ECS Meeting Abstracts* (2019).
10. Hussain, S. *et al.* Fabrication of MoSe2 decorated three-dimensional graphene composites structure as a highly stable electrocatalyst for improved hydrogen evolution reaction. *Renewable Energy* **143**, 1659–1669 (2019).
11. Sata, Y. *et al.* Electric field modulation of Schottky barrier height in graphene/MoSe2 van der Waals heterointerface. *Appl. Phys. Lett.* **107**(2), 023109 (2015).
12. Rehman, M. A. *et al.* Influence of an Al$_2$O$_3$ interlayer in a directly grown graphene-silicon Schottky junction solar cell. *Carbon* **132**, 157–164 (2018).
13. Xue, H. *et al.* A MoSe2/WSe2 heterojunction-based photodetector at telecommunication wavelengths. *Adv. Funct. Mater.* **28**(47), 1804388 (2018).
14. Kozawa, D. *et al.* Evidence for fast interlayer energy transfer in MoSe2/WS2 heterostructures. *Nano Lett.* **16**(7), 4087–4093 (2016).
15. Ye, L., Li, H., Chen, Z. & Xu, J. Near-infrared photodetector based on MoS2/black phosphorus heterojunction. *Acs Photon.* **3**(4), 692–699 (2016).
16. Li, X. *et al.* Two-dimensional GaSe/MoSe2 misfit bilayer heterojunctions by van der Waals epitaxy. *Sci. Adv.* **2**(4), e1501882 (2016).
17. Jeon, P. J. *et al.* Black phosphorus–zinc oxide nanomaterial heterojunction for p–n diode and junction field-effect transistor. *Nano Lett.* **16**(2), 1293–1298 (2016).
18. Naqvi, B. A. *et al.* Visualizing degradation of black phosphorus using liquid crystals. *Sci. Rep.* **8**(1), 12966 (2018).
19. Shehzad, M. A. *et al.* Study of grains and boundaries of molybdenum diselenide and tungsten diselenide using liquid crystal. *Nano Lett.* **17**(3), 1474–1481 (2017).
20. Wang, Z., He, X., Zhang, X. X. & Alshareef, H. N. Hybrid van der Waals p–n heterojunctions based on SnO and 2D MoS2. *Adv. Mater.* **28**(41), 9133–9141 (2016).
21. Xue, F. *et al.* p-type MoS2 and n-type ZnO diode and its performance enhancement by the piezophototronic effect. *Adv. Mater.* **28**(17), 3391–3398 (2016).
22. Amin, B., Singh, N. & Schwingenschlögl, U. Heterostructures of transition metal dichalcogenides. *Phys. Rev. B* **92**(7), 075439 (2015).
23. Mukherjee, B. *et al.* NIR Schottky photodetectors based on individual single-crystalline GeSe nanosheet. *ACS Appl. Mater. Interfaces* **5**(19), 9594–9604 (2013).
24. Novoselov, K. S. *et al.* Two-dimensional atomic crystals. *PNAS* **102**(30), 10451–10453 (2005).
25. Yap, W. C., Yang, Z., Mehboudi, M., Yan, J.-A., Barraza-Lopez, S., Zhu, W. J. N. R. Layered material GeSe and vertical GeSe/MoS 2 pn heterojunctions. **11** (1), 420–430 (2018).
26. Castellanos-Gomez, A. *et al.* Deterministic transfer of two-dimensional materials by all-dry viscoelastic stamping. *2D Mater.* **1**(1), 011002 (2014).

27. Lee, C.-H. *et al.* Atomically thin p–n junctions with van der Waals heterointerfaces. *Nat. Mater.* **9**(9), 676 (2014).
28. Zhang, J. *et al.* Flexible indium–gallium–zinc–oxide Schottky diode operating beyond 2.45 GHz. *Nat. Commun.* **6**(1), 1–7 (2015).
29. Hughes, M., Homewood, K., Curry, R., Ohno, Y. & Mizutani, T. J. A. P. L. An ultra-low leakage current single carbon nanotube diode with split-gate and asymmetric contact geometry. *Appl. Phys. Lett.* **103**(13), 133508 (2013).
30. Aftab, S. *et al.* Formation of an MoTe 2 based Schottky junction employing ultra-low and high resistive metal contacts. *RSC Adv.* **9**(18), 10017–10023 (2019).
31. Dhar, N. *et al.* Effect of N-type transition metal dichalcogenide molybdenum telluride (N-MoTe2) In Back Contact Interface Of Cadmium Telluride Solar Cells From Numerical Analysis. *Chalcogenide Lett.* **11**(6), 1 (2014).
32. Sucharitakul, S. *et al.* Intrinsic electron mobility exceeding 103 cm²/(V s) in multilayer InSe FETs. *Nano Lett.* **15**(6), 3815–3819 (2015).
33. Khalil, H. M. W., Khan, M. F., Eom, J. & Noh, H. Highly stable and tunable chemical doping of multilayer WS2 field effect transistor: Reduction in contact resistance. *ACS Appl. Mater. Interfaces.* **7**(42), 23589–23596 (2015).
34. Khan, M. F. *et al.* High mobility ReSe2 field effect transistors: Schottky-barrier-height-dependent photoresponsivity and broadband light detection with Co decoration. *2D Mater.* **7**(1), 015010 (2019).
35. Sze, S. M., Ng, K. K. *Physics of Semiconductor Devices.* (Wiley, 2006).
36. Abbas, S., Kumar, M. & Kim, J. J. M. S. I. S. P. All metal oxide-based transparent and flexible photodetector. *Mater. Sci. Semiconduct. Process.* **88**, 86–92 (2018).
37. Xie, C. & Yan, F. J. S. Flexible photodetectors based on novel functional materials. *Small* **13**(43), 1701822 (2017).
38. Patel, M. & Kim, J. J. J. O. A. Compounds, transparent NiO/ZnO heterojunction for ultra-performing zero-bias ultraviolet photodetector on plastic substrate. *J. Alloy Compds.* **729**, 796–801 (2017).
39. Abbas, S., Kim, J. J. S. & Physical, A. A. All-metal oxide transparent photodetector for broad responses. *Sens. Actuator A Phys.* **2020**, 11 (1835).
40. Li, L. *et al.* Achieving EQE of 16,700% in P3HT:PC71BM based photodetectors by trap-assisted photomultiplication. *Sci. Rep.* **5**(1), 9181 (2015).
41. Islam, A., Lee, J. & Feng, P.X.-L.J.A.P. Atomic layer GaSe/MoS2 van der waals heterostructure photodiodes with low noise and large dynamic range. *ACS Photon.* **5**(7), 2693–2700 (2018).
42. Hiramoto, M., Imahigashi, T. & Yokoyama, M. Photocurrent multiplication in organic pigment films. *Appl. Phys. Lett.* **64**(2), 187–189 (1994).
43. Abbas, S., Kumar, M., Kim, H.-S., Kim, J. & Lee, J.-H.J.A.A.M. Silver-nanowire-embedded transparent metal-oxide heterojunction Schottky photodetector. *ACS Appl. Mater. Interfaces* **10**(17), 14292–14298 (2018).
44. Monroy, E., Omnès, F. & Calle, F. J. S. S. Wide-bandgap semiconductor ultraviolet photodetectors. *Semicond. Sci. Technol.* **18**(4), R33 (2003).

Acknowledgements

Author contributions

M.H, S.H.A.J, & A.A.: Design, carried out experiments analyzed data and co-wrote paper. D.N.C., J.J., & Y.S.: Performed AFM experiments and analyzed data. S.H., S.A.: Performed low temperature measurements and analyzed data. M.R., & S.Ab.: Co-wrote paper.

Competing interests

The authors declare no competing interests.

Additional information

Supplementary Information The online version contains supplementary material available at https://doi.org/10.1038/s41598-021-83187-z.

Correspondence and requests for materials should be addressed to J.J.

Reprints and permissions information is available at www.nature.com/reprints.

Publisher's note Springer Nature remains neutral with regard to jurisdictional claims in published maps and institutional affiliations.